Supporting Information

Operando Unraveling the Structural/Chemical Stability of P-substituted $CoSe_2$ Electrocatalysts toward Hydrogen/Oxygen Evolution Reactions in Alkaline Electrolyte

Yanping Zhu,[1†] *Hsiao-Chien Chen,*[1,2†] *Chia-Shuo Hsu,*[1] *Ting-Sheng Lin,*[1] *Chia-Jui Chang,*[1] *Sung-Chun Chang,*[3] *Li-Duan Tsai,*[3] *Hao Ming Chen*[1*]

[1]Department of Chemistry, National Taiwan University, Taipei 106, Taiwan

[2]Center of Applied Nanomedicine, National Cheng Kung University, No. 1, University Rd., Tainan 70101, Taiwan.

[3]Materials Chemical Research Laboratories, Industrial Technology Research Institute, Chutung 310, Taiwan.

[†]Contribution equally

1. Experimental Details

1.1 Materials Preparation

Synthesis of cobalt hydroxide carbonate hydrate (CHCH, $Co(OH)(CO_3)_{0.5}{\cdot}xH_2O$ nanowires). In a typical synthesis, the pretreated carbon cloth (CC, 2.5 cm × 1 cm) was perpendicularly immersed into a precursor solution (10 mL) containing 0.625 g of urea and 0.437 g of $Co(NO_3)_3{\cdot}6H_2O$. The immersion depth was kept as 1 cm. Then the aqueous solution and CC were heated at 90 °C for 6 h. After cooling, the CHCH/CC was obtained after being washed with deionized water and dried under vacuum.

Synthesis of phosphorus-substituted cobalt selenide. In a typical synthesis of $CoSe_{1.26}P_{1.42}$, 0.075 g of NaH_2PO_2, 0.06 g of selenium powder and the as-prepared CHCH/CC precursor were placed separately in a glass tube before being heated in a tube furnace at 400 °C for 3 h under a 5% H_2/Ar atmosphere with a temperature ramp of 4 °C min^{-1}. For the synthesis of *c*-$CoSe_2$, $CoSe_{2.01}P_{0.49}$, $CoSe_{1.64}P_{0.54}$ and $CoSe_{0.45}P_{1.18}$,

different amounts of NaH_2PO_2 (0, 0.025, 0.05 and 0.1 g, respectively) were introduced while keeping other parameters unchanged.

1.2 Structure characterization.

The crystallographic information of the samples was evaluated through powder X-ray diffraction (PXRD) analysis (the incident X-ray wavelength of 0.7749 Å) using a large Debye-Scherrer camera in BL-01C2 at National Synchrotron Radiation Research Center (NSRRC, Hsinchu, Taiwan) in which the electron storage ring was operating at 1.5 GeV with a beam current of 360 mA. The XRD patterns were calibrated by CeO_2 standard and altered to that with wavelength of 1.5413 Å using the software "Winplot". The microstructure images were observed with field-emission scanning electron microscope (FE-SEM, JEOL JSM-6700F), transmission electron microscope (TEM) and high-resolution transmission electron microscope (HR-TEM) (JEOL-2100F). Inductively coupled plasma mass spectrometry (ICP-MS) was performed on iCAP-RQ instrument (Thermo Fisher). Typically, the samples were dissolved in 2 wt% HNO_3 and the ion concentration is kept less than 50 ppb. X-ray absorption spectroscopy at Co K-edge were collected in total-fluorescence-yield mode at ambient air in BL-01C1 at NSRRC. The scan range was kept in an energy range of 7600-8300 eV for Co K-edge. The spectra were obtained after subtracting the baseline of pre-edge and normalizing that of post-edge. In situ Raman spectra were recorded by UniNano UNIDRON. A Raman microscopy system, employing a diode laser at 532 nm. A 50× objective lens was used to focus the laser on the sample, in which the size of laser spot is 1 μm. Meanwhile the Raman spectrum measurement was performed under an exposure time of 2 s and an accumulation number of 5 times by illuminating 2.5 mW laser power.

1.3 Electrochemical measurements.

Electrochemical performance was assessed on a Bio-Logic SP-300 workstation at RT. All tests were carried out in 1 M potassium hydroxide (KOH) electrolyte in a conventional three-electrode configuration. Reference electrode: saturated calomel electrode (SCE). Counter electrode: graphite rod for HER and platinum plate for OER. Working electrode: the as-prepared catalysts. All the potentials reported were

referenced *vs* reversible hydrogen electrode (RHE) according to the equation with IR compensation: E(RHE) = E(SCE) + 0.059 × pH + 0.240. The working area of electrodes was fixed as 0.5 cm^2. For the HER test, Polarization curves were recorded using linear sweep voltammetry (LSV) from -0.8 to -1.6 V (vs SCE) at a sweep rate of 5 mV s^{-1}. The cyclic voltammograms(CVs) obtained with different rates from 2 to 10 mV s^{-1} in the potential range of -0.4 - -0.45 V (vs. RHE) were recorded to calculate the electrochemical double-layer capacitances (EDLCs), $C_{dl.}$ The long-term stability was tested under a static overpotential of 92 mV for 15 hours. For the OER test, LSV was recorded under the potential window ranged from 0 to 0.8 V (vs SCE) and the scanning rate was 0.5 mV s^{-1}. The overpotential (η) was obtained based on the equation: E(RHE) - 1.23 V = η (V). Cyclic voltammograms (CVs) tests were carried out in the potential window of 0.15 - 0.2 V (vs. SCE) with different sweeping rates from 0.2 to 1 mV s^{-1} to calculate EDLCs, C_{dl}. The long-term stability was tested under a static overpotential of 255 mV for 15 hours.

1.4 *In-Situ* X-ray absorption spectroscopy analysis

The measurement in a typical three-electrode setup as the same condition in electrochemical characterization case was performed in a specially designed Teflon container with a window sealed by Kapton tape. X-ray was allowed to transmit through the tape and electrolyte, so that the signal of X-ray absorption spectroscopy could be collected in total-fluorescence-yield mode in TPS BL-44A in NSRRC.

2. Supplymentary Results

Figure S1 Photograph of the synthesis of the P-substituted $CoSe_2$ nanostructures on CC.

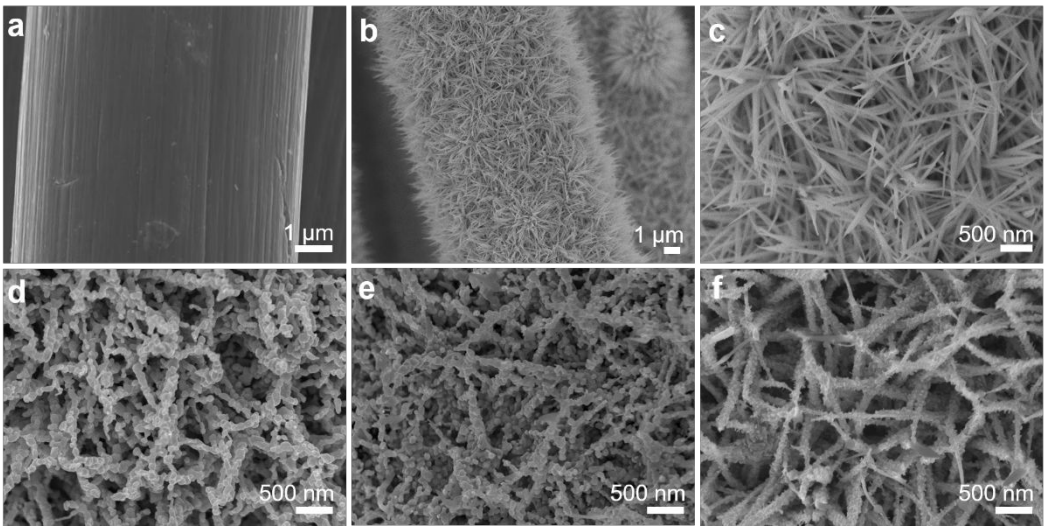

Figure S2 (a) SEM image of bare CC. (b) Low and (c) high magnification SEM images of the CHCH precursor. SEM images of (d) $CoSe_{2.01}P_{0.49}$, (e) $CoSe_{1.64}P_{0.54}$ and (f) $CoSe_{0.45}P_{1.18}$.

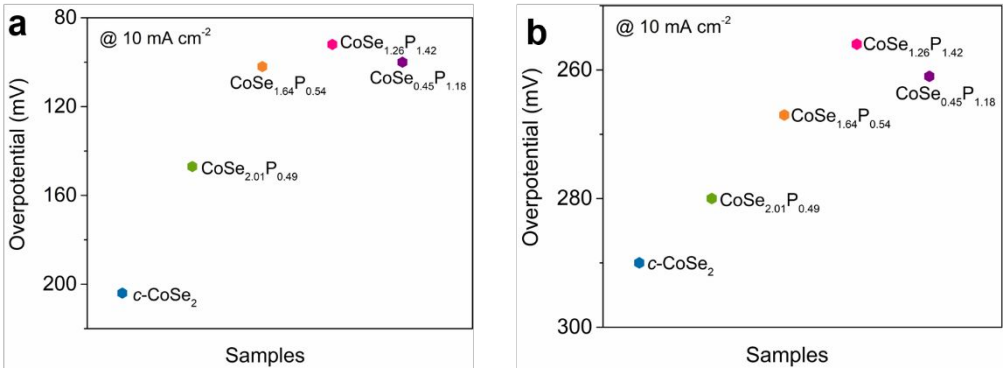

Figure S3. Volcano plots obtained from (a) HER and (b) OER performance of the catalysts.

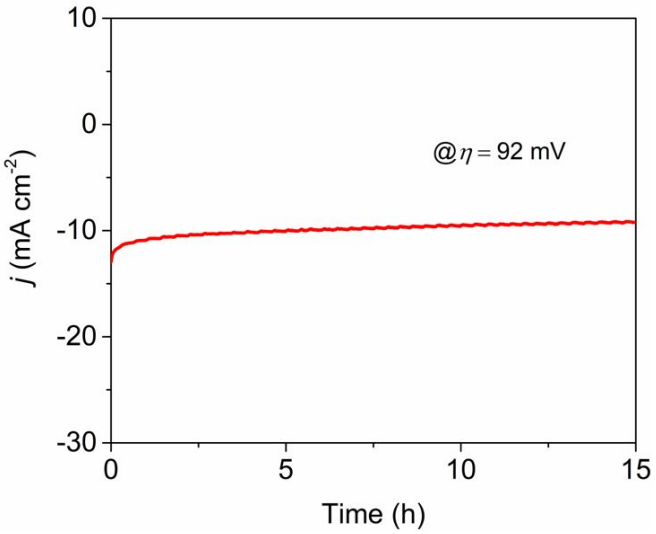

Figure S4. Current density as a function of time for $CoSe_{1.26}P_{1.42}$ at a constant cathodic potential of 92 mV toward HER.

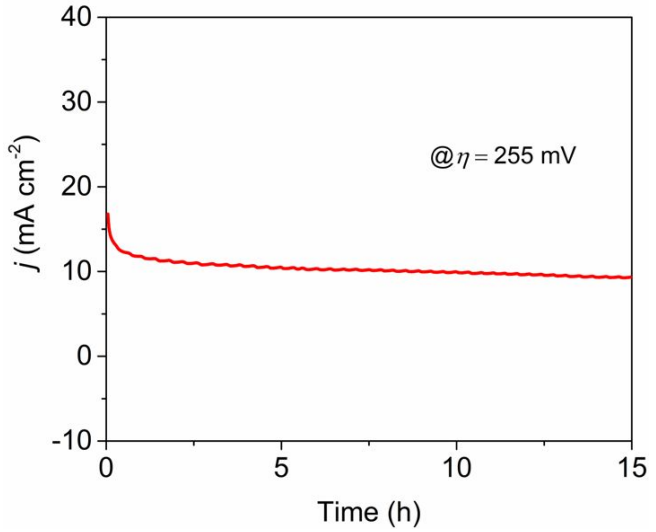

Figure S5. Current density as a function of time for $CoSe_{1.26}P_{1.42}$ at a constant overpotential of 255 mV toward OER.

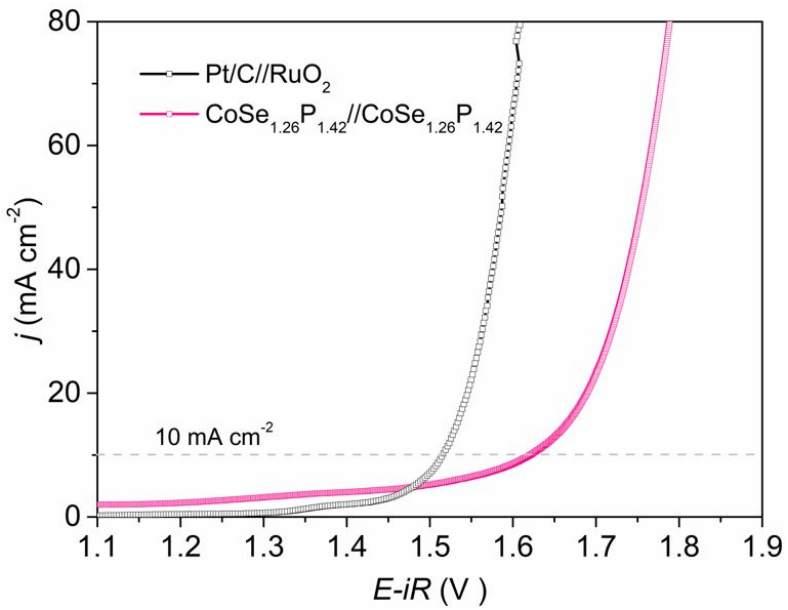

Figure S6. (a) Polarization curves of $CoSe_{1.26}P_{1.42}$//$CoSe_{1.26}P_{1.42}$ and Pt/C//RuO_2 for overall water splitting in 1 M KOH.

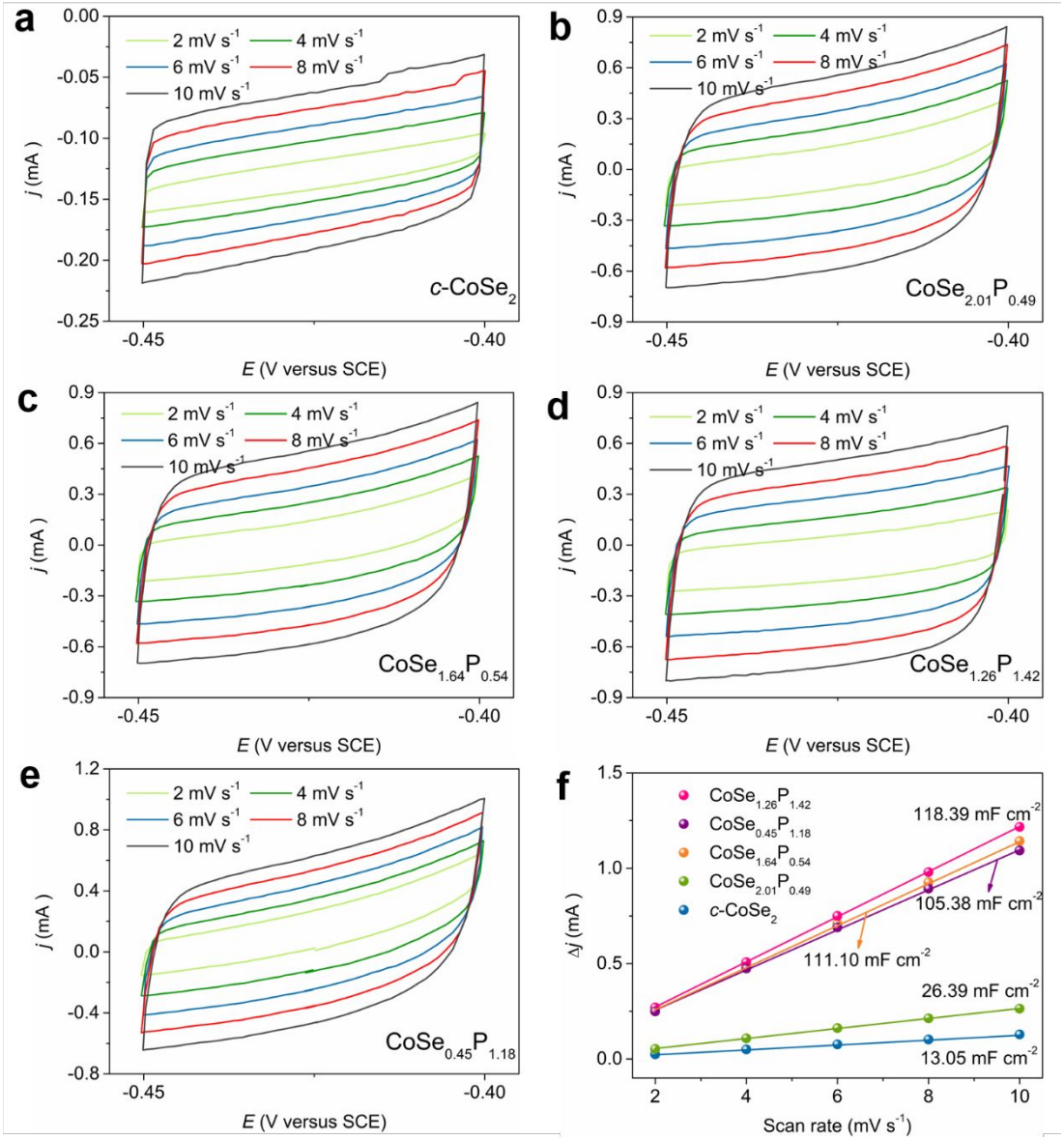

Figure S7. CV curves recorded for (a) *c*-$CoSe_2$, (b) $CoSe_{2.01}P_{0.49}$, (c) $CoSe_{1.64}P_{0.54}$, (d) $CoSe_{1.26}P_{1.42}$ and (e) $CoSe_{0.45}P_{1.18}$ catalysts at 2 - 10 mV S^{-1} in the potential range of -0.45 V ~ -0.40 V SCE. (f) The corresponding linear fitting of the capacitive currents versus CV scans.

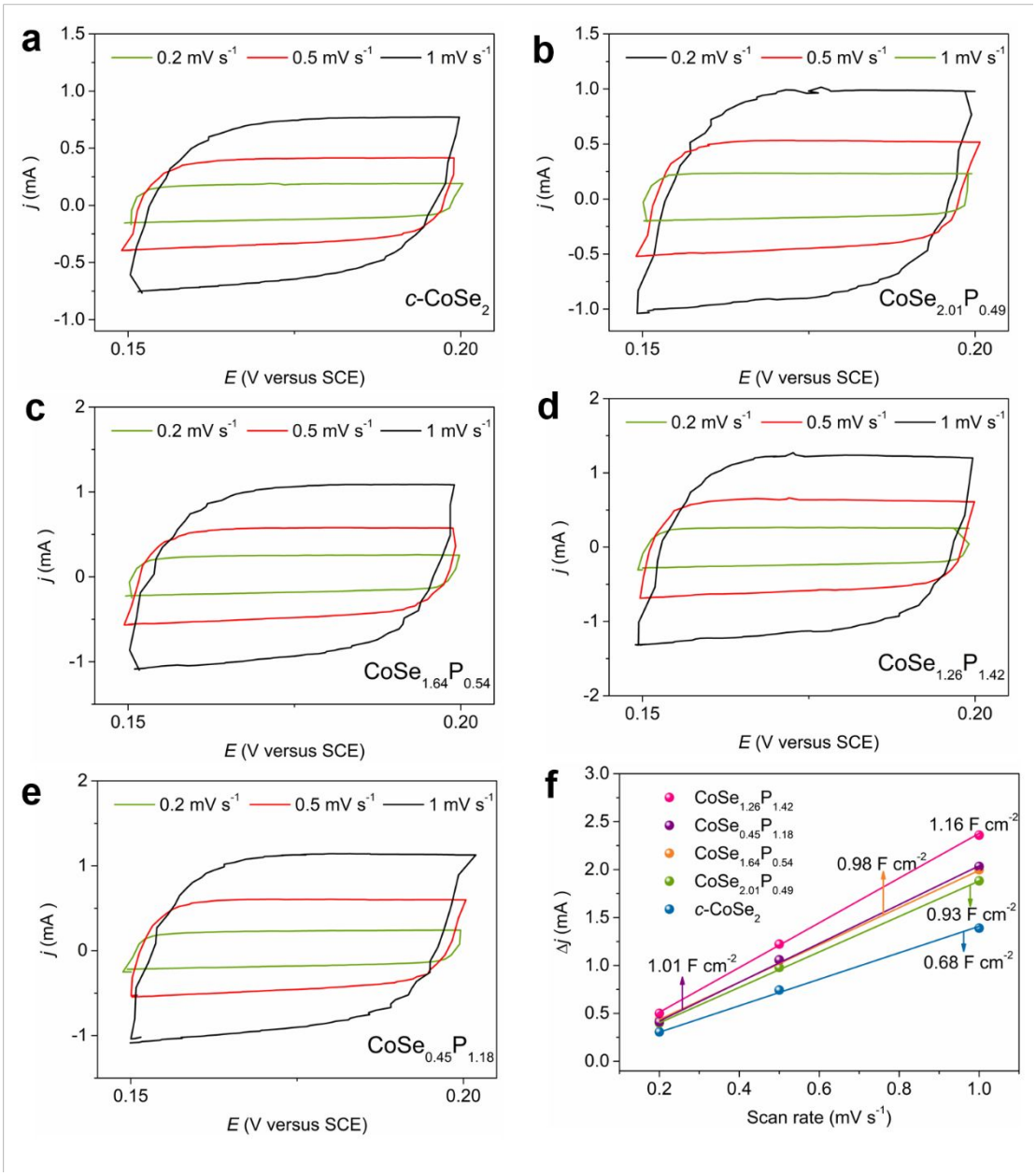

Figure S8. CV curves recorded for (a) *c*-$CoSe_2$, (b) $CoSe_{2.01}P_{0.49}$, (c) $CoSe_{1.64}P_{0.54}$, (d) $CoSe_{1.26}P_{1.42}$ and (e) $CoSe_{0.45}P_{1.18}$ catalysts at 0.2 ~ 1 mV s^{-1} in the potential range of 0.15 V ~ 0.2 V SCE. (f) The corresponding linear fitting of the capacitive currents versus CV scans.

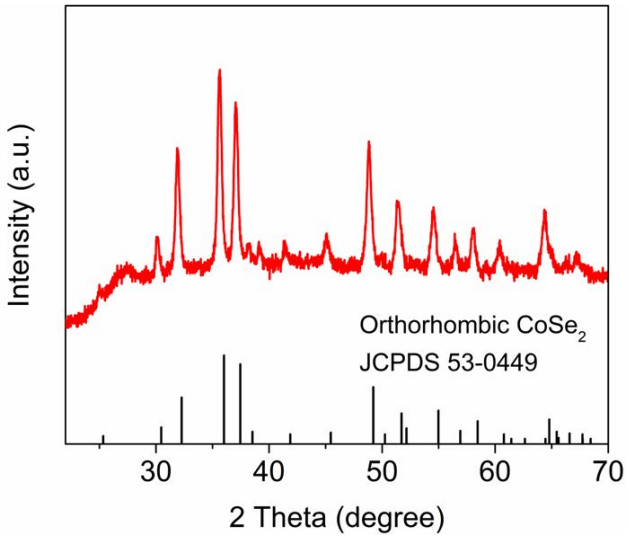

Figure S9. XRD pattern of the *o*-$CoSe_2$.

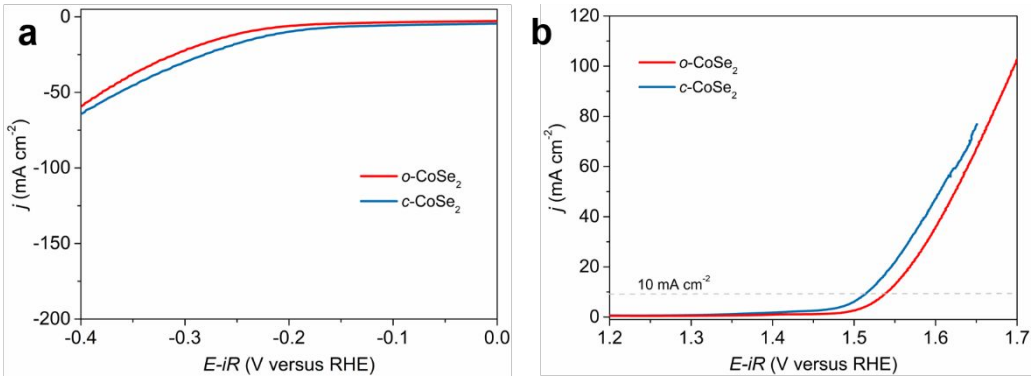

Figure S10. Electrochemical activity comparison between the *o*-$CoSe_2$ and *o*-$CoSe_2$ electrode: LSV polarization curves for (a) HER and (b) OER.

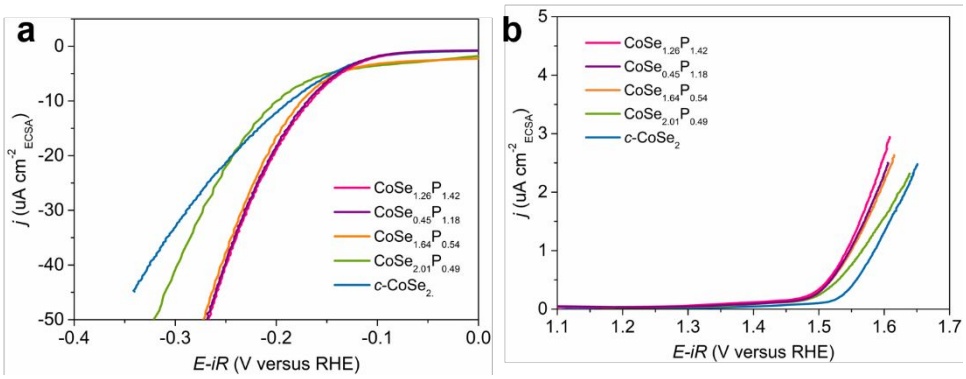

Figure S11. (a) HER and (b) OER polarization curves of the catalysts normalized by ECSA.

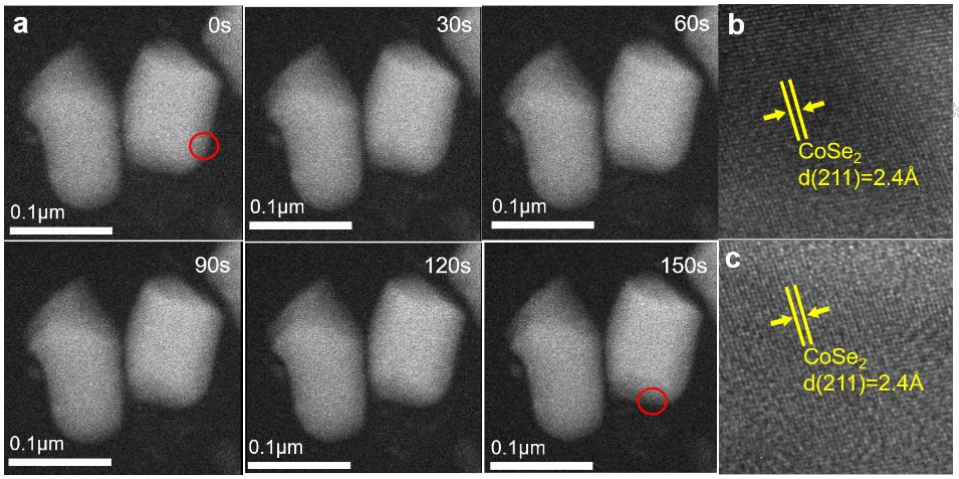

Figure S12. (a) *In-situ* STEM images of the *c*-$CoSe_2$ catalyst taken at different times after immersing into the KOH solution. HRTEM images of the selected region of (b) initial and (c) final state of the *c*-$CoSe_2$.

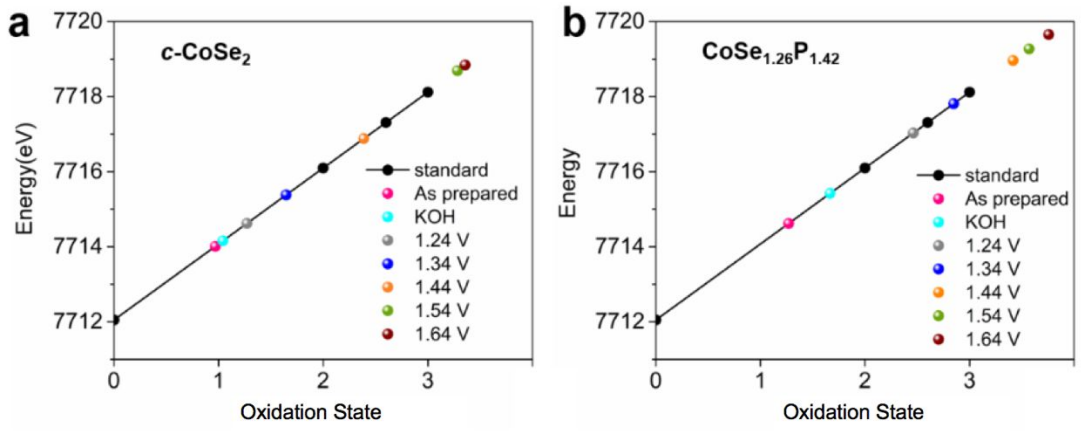

Figure S13. The oxidation states of cobalt of (a) *c*-$CoSe_2$ and (b) $CoSe_{1.26}P_{1.42}$ at various potentials for the OER process.

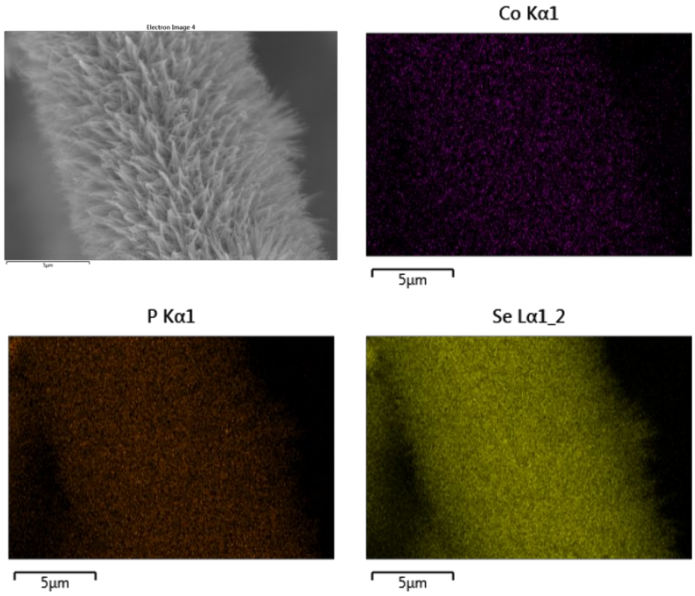

Figure S14. EDX elemental mapping of the as-prepared $CoSe_{1.26}P_{1.42}$.

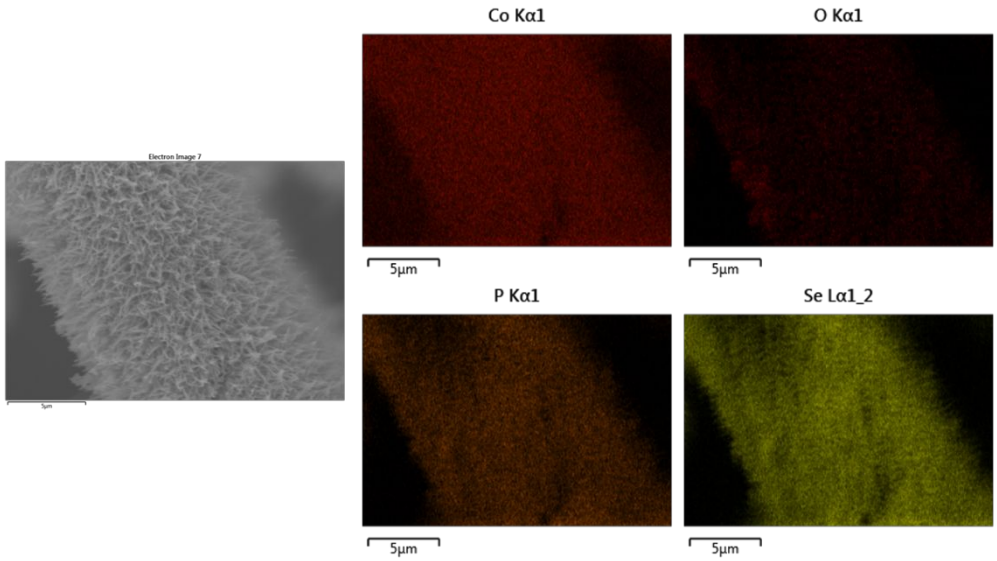

Figure S15. EDX elemental mapping of the $CoSe_{1.26}P_{1.42}$ after HER.

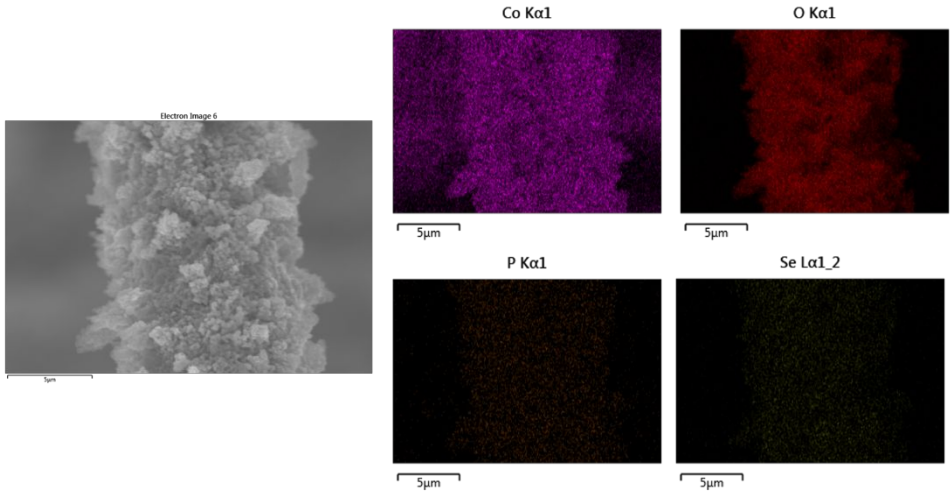

Figure S16. EDX elemental mapping of the $CoSe_{1.26}P_{1.42}$ after OER.

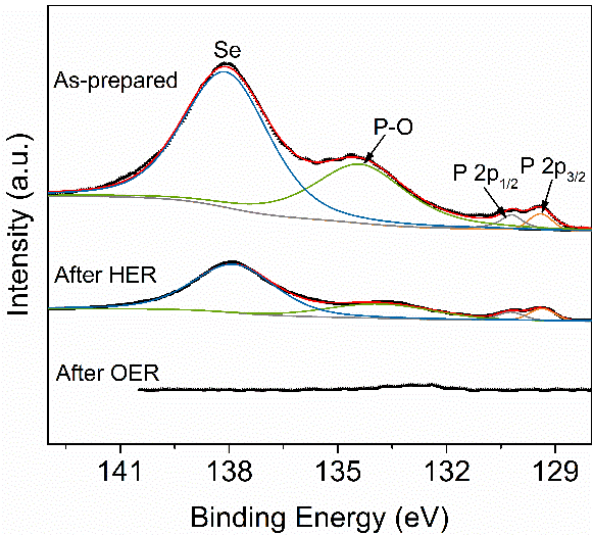

Figure S17. XPS spectra of P 2p of the $CoSe_{1.26}P_{1.42}$ before and after HER/OER.

For the P 2p spectrum of the as-prepared $CoSe_{1.26}P_{1.42}$, the peaks at 129.4 and 130.2 eV reflect the binding energies of P $2P_{3/2}$ and P $2P_{1/2}$, respectively. The peak at 134.4 eV is assigned to the surface PO_4 due to the air exposure (*J. Mater. Chem. A*, **2016**, *4*, 4686-4690), which may affect the resultant coordination numbers of Co. The additional peak located at 187.1 eV represents the Auger Se.

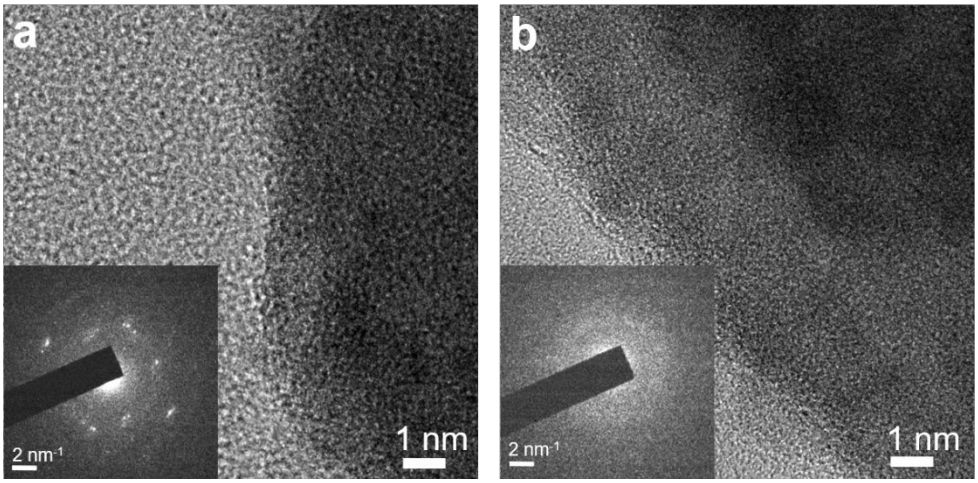

Figure S18. TEM images of the $CoSe_{1.26}P_{1.42}$ catalyst after (a) HER and (b) OER stability test. Insets are the corresponding SAED pattern.

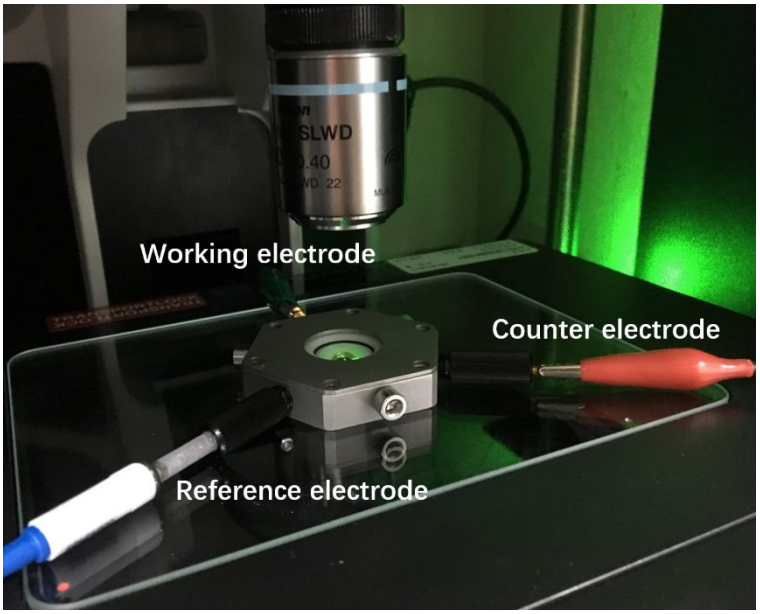

Figure S19. Digital photograph of the chemical cell for using in *in-situ* Raman measurement.

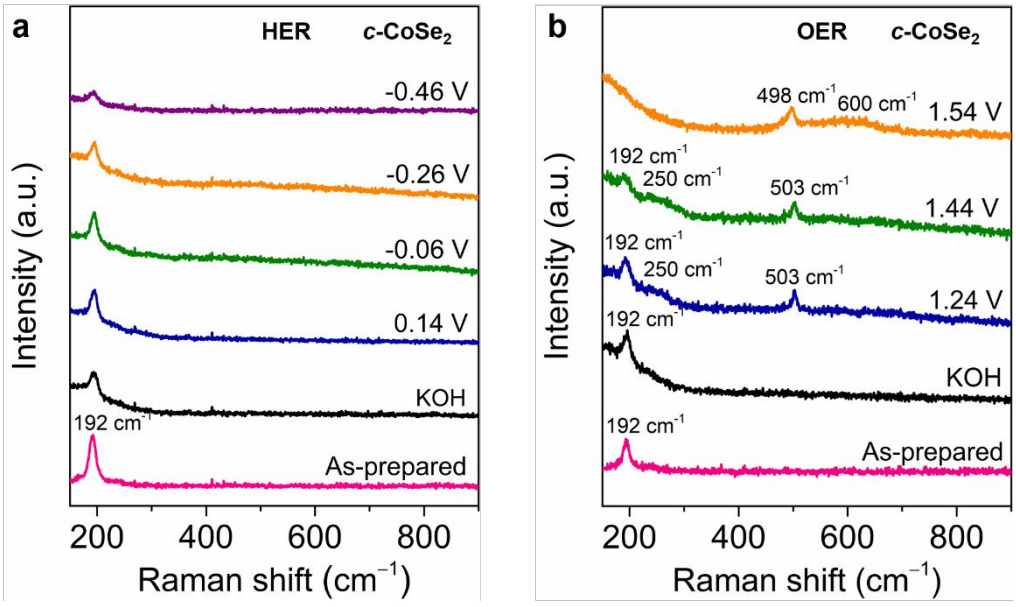

Figure S20. *In-situ* Raman spectra of the *c*-$CoSe_2$ catalyst at various potentials for (a) HER and (b) OER process.

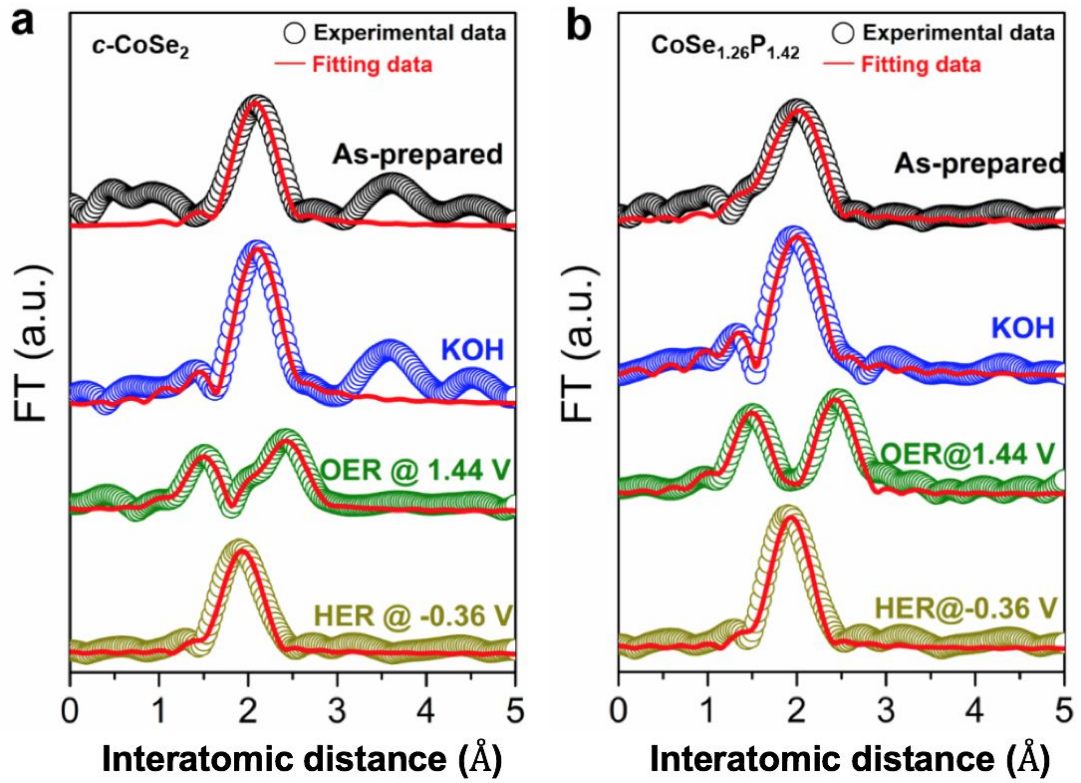

Figure S21. *In-situ* EXAFS r-space spectra of (a) *c*-$CoSe_2$ and (b) $CoSe_{1.26}P_{1.42}$ catalysts for HER and OER process. (experimental data; color circle) and the corresponding fitting (red line).

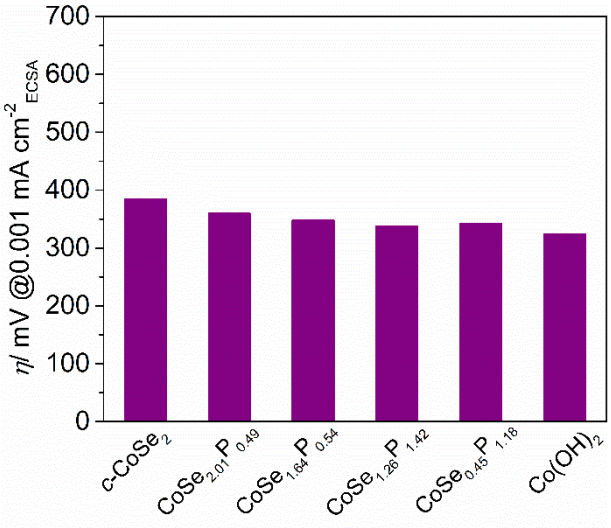

Figure S22. ECSA normalized activity of all samples and reference $Co(OH)_2$.

Table S1. Compositions of the samples determined from ICP-MS.

Samples	The mole ratios of metal ions		
	Co	Se	P
c-$CoSe_2$	1	2.13	/
$CoSe_{2.01}P_{0.49}$	1	2.01	0.49
$CoSe_{1.64}P_{0.54}$	1	1.64	0.54
$CoSe_{1.26}P_{1.42}$	1	1.26	1.42
$CoSe_{0.45}P_{1.18}$	1	0.45	1.18

Table S2. Comparison of electrocatalytic HER activity in alkaline media (1 M KOH) for $CoSe_{1.26}P_{1.42}$ with some of the most active non-precious HER catalysts ever reported.

Catalyst	Substrate	η_{10} (mV)	Tafel slope (mV dec^{-1})	Reference
$CoSe_{1.26}P_{1.42}$	CC	92	90	This work
CoP	CC	41	43	[1]
NiS_2	CC	149	104	[2]
MoP-NC/MoP-C	CC	69	50	[3]
Ni-thiolate	CC	80	70	[4]
Ni/NiO	Ni Foam	146	72	[5]
Ni-Fe-P	Ni Foam	79	93	[6]
Co/Co_2P	Ni Foam	124	60	[7]
$Pr_{0.5}$BSCF	GCE	237	45	[8]
o-$CoSe_2$|P	GCE	104	69	[9]
N_i-Mo_2C-PC	GCE	169	101	[10]
C_OO_x@CN	GCE	235	115	[11]

Table S3. Comparison of electrocatalytic OER activity in alkaline media (1 M KOH) for $CoSe_{1.26}P_{1.42}$ with some of the most active non-precious OER catalysts ever reported.

Catalyst	Substrate	η_{10} (mV)	Tafel slope (mV dec^{-1})	Reference
$CoSe_{1.26}P_{1.42}$	CC	255	87	This work
$CoSe_{0.85}$	CC	324	85	[12]
NiCoPS	CC	230	45	[13]
NiCoP	CC	242	64	[14]
Ni_3S_2	Ni foam	157	59	[15]
FeNi-GO LDH	Ni foam	210	40	[16]
Ni_2P	Ni foam	290	59	[17]
p-$Cu_{1-x}NNi_{3-y}$/FeNiCu	GCE	280	52	[18]
Co_4N	GCE	330	58	[19]
Ni_3N nanosheets	GCE	350	85	[20]
CoMnP	GCE	330	61	[21]
$SCFW_{0.4}$	GCE	296	50	[22]
Amorphous CoSe film	Ti mesh	292	69	[23]

Table S4. Compositions of the catalysts after reaction determined from ICP-MS.

Samples	The mole ratios of metal ions		
	Co	Se	P
c-$CoSe_2$-HER	1	0.75	/
$CoSe_{1.26}P_{1.42}$-HER	1	0.38	0.49
c-$CoSe_2$-OER	1	0.08	/
$CoSe_{1.26}P_{1.42}$-OER	1	0.03	0.11

References

1. Yang, X.; Lu, A.; Zhu, Y.; Hedhili, M.; Min, S.; Huang, K.; Han, Y.; Li, L. CoP Nanosheet Assembly Grown on Carbon Cloth: A Highly Efficient Electrocatalyst for Hydrogen Generation. *Nano Energy* **2015**, *15*, 634-641.
2. Tang, C.; Pu, Z.; Liu, Q.; Asiri, A.; Sun, X. NiS_2 Nanosheets Array Grown on Carbon Cloth as An Efficient 3D Hydrogen Evolution Cathode. *Electrochimica Acta* **2015**, *153*, 508-514.
3. Liu, B.; Li, H.; Cao, B.; Jiang, J.; Gao, R.; Zhang, J. Few Layered N, P Dual-Doped Carbon-Encapsulated Ultrafine MoP Nanocrystal/MoP Cluster Hybrids on Carbon Cloth: An Ultrahigh Active and Durable 3D Self-Supported Integrated Electrode for Hydrogen Evolution Reaction in a Wide pH Range. *Adv. Mater.* **2018**, *28*, 1801527.
4. Hu, C.; Ma, Q.; Hung, S.; Chen, Z.; Ou, D.; Ren, B.; Chen, H.; Fu, G.; Zheng, N. In Situ Electrochemical Production of Ultrathin Nickel Nanosheets for Hydrogen Evolution Electrocatalysis. *Chem* **2017**, *3*, 122-133.
5. Sun, H.; Ma, Z.; Qiu, Y.; Liu, H.; Gao, G. Ni@NiO Nanowires on Nickel Foam Prepared via "Acid Hungry" Strategy: High Supercapacitor Performance and Robust Electrocatalysts for Water Splitting Reaction. *Small* **2018**, *14*, 1800294.
6. Ahn, S.; Manthiram, A. Direct Growth of Ternary Ni-Fe-P Porous Nanorods onto Nickel Foam as A Highly Active, Robust Bi-Functional Electrocatalyst for Overall Water Splitting. *J. Mater. Chem. A* **2017**, *5*, 2496-2503.
7. Masa, J.; Barwe, S.; Andronescu, C; Sinev, I.; Ruff, A.; Jayaramulu, K.; Elumeeva, K.; Konkena, B.; Cuenya, B.; Schuhmann, W. Low Overpotential Water Splitting Using Cobalt-Cobalt Phosphide Nanoparticles Supported on Nickel Foam. *ACS Energy Lett.* **2016**, *1*, 1192-1198.
8. Xu, X.; Chen, Y.; Zhou, W.; Zhu, Z.; Su, C.; Liu, M.; Shao, Z. A Perovskite Electrocatalyst for Efficient Hydrogen Evolution Reaction. *Adv. Mater.* **2016**, *28*, 6442-6448.
9. Zheng, Y.; Wu, P.; Gao, M.; Zhang, X.; Gao, F.; Ju, H.; Wu, R.; Gao, Q.; You, R.; Huang, W. *et al.* Doping-Induced Structural Phase Transition in Cobalt Diselenide Enables Enhanced Hydrogen Evolution Catalysis. *Nat. Commun*. **2018**, *9*, 2533.
10. Yu, Z.; Duan, Y.; Gao, M.; Lang, C.; Zheng, Y.; Yu, S. A One-Dimensional Porous Carbon-Supported Ni/Mo_2C Dual Catalyst for Efficient Water Splitting. *Chem. Sci.* **2017**, *8*, 968-973.
11. Jin, H.; Wang, J.; Su, D.; Wei, Z.; Pang, Z.; Wang, Y. In Situ Cobalt-Cobalt Oxide/N-Doped Carbon Hybrids as Superior Bifunctional Electrocatalysts for Hydrogen and Oxygen Evolution. *J. Am. Chem. Soc.* **2015**, *137*, 2688-2694.
12. Xia, C., Jiang, Q., Zhao, C., Hedhili, M.; Alshareef, H. Selenide-Base Electrocatalysts and Scaffolds for Water Oxidation Applications. *Adv. Mater.* **2016**, *28*, 77-85.
13. Li, J.; Xia, Z.; Zhou, X.; Qin, Y.; Ma, Y.; Qu, Y. Quaternary Pyrite-Structured Nickel/Cobalt Phosphosulfide Nanowires on Carbon Cloth as Efficient and Robust Electrodes for Water Electrolysis. *Nano Research* **2017**, *10*, 814-825.

14. Du, C.; Yang, L.; Yang, F.; Cheng, G.; Luo, W. Nest-Like NiCoP for Highly Efficient Overall Water Splitting. *ACS Catal.* **2017**, *7*, 4131-4137.
15. Zhou, W.; Xu, X.; Cao, X.; Huang, X.; Tan, C.; Tian, J.; Liu, H.; Wang, J.; Zhang, H. Ni_3S_2 Nanorods/Ni Foam Composite Electrode with Low Overpotential for Electrocatalytic Oxygen Evolution. *Energy Environ. Sci.* **2013**, *6*, 2921-2924.
16. Long, X.; Li, J.; Xiao, S.; Yan, K.; Wang, Z.; Chen, H.; Yang, S. A Strongly Coupled Graphene and FeNi Double Hydroxide Hybrid as An Excellent Electrocatalyst for the Oxygen Evolution Reaction. *Angew. Chem. Int. Ed.* **2014**, *126*, 7714-7718.
17. Stern, L.; Feng, L.; Song, F.; Hu, X. Ni_2P as A Janus Catalyst for Water Splitting: The Oxygen Evolution Activity of Ni_2P Nanoparticles. *Energy Environ. Sci.* **2015**, *8*, 2347-2351.
18. Zhu, Y.; Chen, G.; Zhong, Y.; Chen, Y.; Ma, N.; Zhou, W.; Shao, Z. A Surface-Modified Antiperovskite as An Electrocatalyst for Water Oxidation. *Nat. Commun.* **2018**, *9*, 2326.
19. Xu, K.; Chen, P.; Li, X.; Tong, Y.; Ding, H.; Wu, X.; Chu, W.; Peng, Z.; Wu, C.; Xie, Y. Metallic Nickel Nitride Nanosheets Realizing Enhanced Electrochemical Water Oxidation. *J. Am. Chem. Soc.* **2015**, *137*, 4119-4125.
20. Zhang, Y.; Ouyang, B.; Xu, J.; Jia, G.; Shen, S.; Rawat, R.; Fan, H. Rapid Synthesis of Cobalt Nitride Nanowires: Highly Efficient and Low-Cost Catalysts for Oxygen Evolution. *Angew. Chem. Int. Ed.* **2016**, *55*, 8670-8674.
21. Li, D.; Baydoun, H.; Verani, C.; Brock, S. Efficient Water Oxidation Using CoMnP Nanoparticles. *J. Am. Chem. Soc.* **2016**, *138*, 4006-4009.
22. Chen, G.; Hu, Z.; Zhu, Y.; Chen, Z.; Zhong, Y.; Lin, H.; Chen, C.; Tjeng, L.; Zhou, W.; Shao, Z. Ultrahigh-Performance Tungsten-Doped Perovskites for the Oxygen Evolution Reaction. *J. Mater. Chem. A* **2018**, *6*, 9854-9859.
23. Liu, T.; Liu, Q.; Asiri, A.; Luo, Y.; Sun, X. An Amorphous CoSe Film Behaves as An Active and Stable Full Water-Splitting Electrocatalyst under Strongly Alkaline Conditions. *Chem. Commun.* **2015**, *51*, 16683-16686.